

# RSC Advances



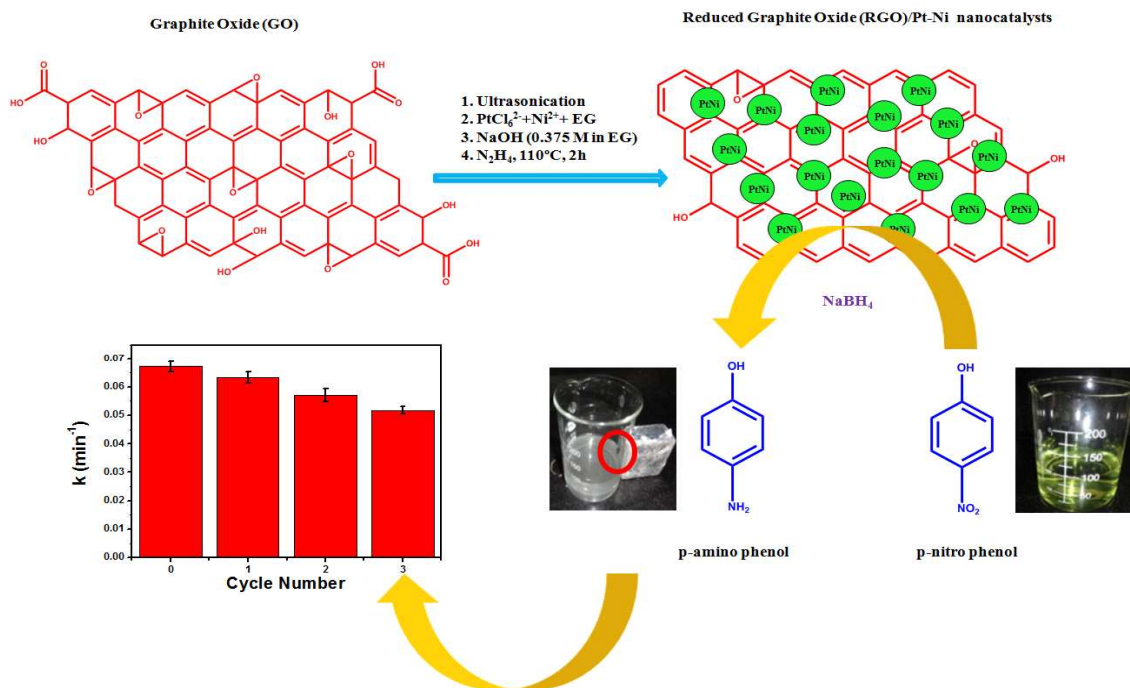
This is an *Accepted Manuscript*, which has been through the Royal Society of Chemistry peer review process and has been accepted for publication.

*Accepted Manuscripts* are published online shortly after acceptance, before technical editing, formatting and proof reading. Using this free service, authors can make their results available to the community, in citable form, before we publish the edited article. This *Accepted Manuscript* will be replaced by the edited, formatted and paginated article as soon as this is available.

You can find more information about *Accepted Manuscripts* in the [Information for Authors](#).

Please note that technical editing may introduce minor changes to the text and/or graphics, which may alter content. The journal's standard [Terms & Conditions](#) and the [Ethical guidelines](#) still apply. In no event shall the Royal Society of Chemistry be held responsible for any errors or omissions in this *Accepted Manuscript* or any consequences arising from the use of any information it contains.

Synthesis of RGO/Pt-Ni nanocatalysts and catalytic reduction of p-nitrophenol by using as synthesized nanocatalysts (Magnetic separation and Recycling)



## Facile synthesis of Reduced Graphene Oxide/Pt-Ni nanocatalysts: Its magnetic and catalytic properties

Prasanta Kumar Sahoo,<sup>a</sup> Bharati Panigrahy,<sup>b</sup> and Dharendra Bahadur.<sup>a\*</sup>

The catalytic performance of metals can be enhanced by intimately alloying different metals with Reduced Graphene Oxide (RGO). In this work, we have demonstrated a simplistic in situ one-step reduction approach for the synthesis of RGO/Pt-Ni nanocatalysts with different atomic ratios of Pt and Ni, without using any capping agents. The physical properties of the as-synthesized nanocatalysts have been systematically investigated by XRD, FTIR, Raman spectroscopy, XPS, EDX, ICP-AES, and TEM. The composition dependent magnetic properties of the RGO/Pt-Ni nanocatalysts were investigated at 5 and 300 K, respectively. The results confer that the RGO/Pt-Ni nanocatalysts show super-paramagnetic nature at room temperature in all compositions. Furthermore, the catalytic activities of the RGO/Pt-Ni nanocatalysts were investigated by analyzing the reduction of p-nitrophenol and it is found that the reduction rate is susceptible to a composition of Pt and Ni. Moreover, it has been found that RGO/Pt-Ni nanocatalysts show superior catalytic activity as compared to the bare Pt-Ni of same composition. Interestingly, the nanocatalysts can be readily recycled by a strong magnet and reused for the next reactions.

### 1. Introduction

Recently, graphene, a two-dimensional material of one-atom thick sheet of carbon has grabbed the attention of many scientists. This exciting material shows outstanding thermal, mechanical and electrical properties, which make it a potential material for possible applications in various fields.<sup>1</sup> Triggered by these extraordinary properties,<sup>2</sup> the attention towards graphene has expanded to many areas of chemical applications including adsorption and photocatalysis,<sup>3,4</sup> heterogeneous catalysis<sup>5</sup> and biosensors.<sup>6</sup> Properties such as high solubility, high surface area and no mass transfer barriers make this material very suitable in catalysis as a new form of carbon material.<sup>7-9</sup> So far, graphene sheets have been prepared by several techniques like micromechanical exfoliation, UV assisted processing,<sup>10</sup> thermal expansion of graphite,<sup>11</sup> chemical vapor deposition<sup>12</sup> and solution-based chemical reduction of exfoliated graphite oxide.<sup>13, 14</sup> Among them, solution-based chemical reduction of exfoliated graphite oxide (GO) is both easily scalable and affording technique for large-scale production of graphene sheets. Some of the current studies on graphene-based nanocomposites have shown that a synergistic combination of metal, metal oxide nanoparticles with graphene sheets enhances their properties and performances, which make them use in various fields of promising application.<sup>15,16</sup> Particularly the integration of magnetic nanoparticles with graphene sheets is used in many potential applications in the fields of energy and information storage,<sup>17,18</sup> magnetic

resonance imaging,<sup>19</sup> targeted drug carriers,<sup>20</sup> water purification<sup>21</sup> and catalysis.<sup>22</sup>

Last few decades, alloying of two kinds of metal nanoparticles has great interest because of their exceptional electronic,<sup>23</sup> optical,<sup>24</sup> and catalytic properties.<sup>25</sup> over the respective individual metal nanoparticles. For example, Y. Huang et al. has reported that Pt-Ni nanocrystals show much better performance and durability than the commercial Pt black and commercial Pt/C catalysts for oxygen reduction reaction.<sup>26</sup> Recently, it has been demonstrated that graphene-supported metal alloys like Ni-Co,<sup>27</sup> Zn-Ni,<sup>28</sup> Fe-Pt,<sup>29</sup> Fe-Ni<sup>30</sup> and Pt-Ni<sup>31</sup> exhibit unusually high catalytic performance, which makes graphene an ideal substitute for other carbon materials as catalyst support. Since the reduction of aromatic nitro compounds to amine is a very vital process in the synthetic organic chemistry and in the industry for the fabrication of industrial products. Hence, the development of an effective, environmentally friendly and recyclable catalyst is anticipated for the reduction of aromatic nitro compounds to amine. Now a day's reduction of p-nitro phenol to p-amino phenol by NaBH<sub>4</sub> has been widely used as a model reaction for quantify the catalytic activity of various metal or alloy catalysts. For instance, T. Pal et al. has reported that Pt-Ni bi metallic nanoparticles show superior catalytic activity in the borohydrate reduction of p-nitro phenol than monometallic Pt nanoparticles of comparable sizes.<sup>32</sup> In the present work, the RGO/Pt-Ni nanocatalysts, with different ratios of Pt and Ni have been synthesized by a simple,

one-step reduction approach. The structural and magnetic properties of as-synthesized nanocatalysts were studied. The catalytic studies for the p-nitro phenol reduction by RGO/Pt-Ni nanocatalysts with varying ratios of Pt and Ni have been undertaken. Its magnetic studies help in understanding its potential for the separation of these precious catalysts. The catalytic activity of RGO/Pt-Ni nanocatalyst has been compared with that of bare Pt-Ni, RGO/Ni and RGO/Pt nanocatalysts as well as some other reported Bi-metallic and RGO/Bi-metallic systems.<sup>27,28,33,34</sup> The results obviously indicate the excellent catalytic activity of RGO/Pt-Ni nanocatalysts toward the reduction of p-nitrophenol as compared to bare Pt-Ni, RGO/Ni, RGO/Pt and other reported Bi-metallic and RGO/Bi-metallic systems.

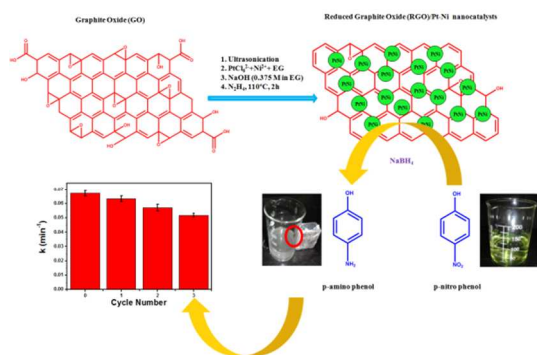
## 2. Experimentation and characterization

### 2.1 Materials

Graphite powder with a particle size of 45  $\mu\text{m}$  (99.99 % purity), hexachloroplatinate ( $\text{H}_2\text{PtCl}_6 \cdot 6\text{H}_2\text{O}$ ) and nickel(II) nitrate hexahydrate ( $\text{Ni}(\text{NO}_3)_2 \cdot 6\text{H}_2\text{O}$ ) were purchased from Sigma-Aldrich. All other chemicals used in our experiments were ordered from Merck Specialties Private Limited, India, and were used as-received, without further purification.

### 2.2 Preparation of RGO/Pt-Ni nanocatalysts

Graphite Oxide (GO) was prepared from graphite powder by modified Hummers method.<sup>35</sup> RGO/Pt-Ni nanocatalysts were synthesized by a one step chemical reduction method in the absence of capping agents. In a typical synthesis, 35 mg of GO was added to 80 mL ethylene glycol (EG) and ultrasonicated for 1 h to form a stable colloid of graphene oxide. The required amount of  $\text{H}_2\text{PtCl}_6 \cdot 6\text{H}_2\text{O}$  and  $\text{Ni}(\text{NO}_3)_2 \cdot 6\text{H}_2\text{O}$  were dissolved in 20 mL of EG. This salt solution was added to the suspension of GO. Consequently, 0.8 mL of hydrazine hydrate (85 wt %) and 3.6 mL of 0.375 M NaOH (made with EG) were added and this mixture was kept in an ultrasonic bath for 10 minutes. Then this mixture was heated at 110  $^\circ\text{C}$  for 3 h under  $\text{N}_2$  atmosphere. The reaction mixture was cooled and subsequently separated by centrifugation. The synthesized solid products were thoroughly washed with milli-Q water and absolute ethanol. It was then dried in a vacuum oven at 50  $^\circ\text{C}$  for 24 h.<sup>36</sup> A schematic diagram showing details of the synthesis process is presented in the Scheme 1.



**Scheme 1** Schematic presentation for the synthesis of reduced graphene oxide (RGO)/Pt-Ni nanocatalysts by single-step chemical reduction method and catalytic reduction of p-nitro phenol into p-amino phenol by  $\text{NaBH}_4$  in presence of as synthesized nanocatalysts (Magnetic separation and Recycling).

RGO/Pt-Ni nanocatalysts with different Pt and Ni atomic ratios of 25:75; 33:67 and 50:50 were synthesized by adjusting the amount of the respective metal salts, keeping the GO amount constant (35 mg) in all cases. The total loading amount of Pt

and Ni (Pt:Ni) in RGO/Pt-Ni (25:75), RGO/Pt-Ni (33:67) and RGO/Pt-Ni (50:50) was controlled so that it was approximately 40 wt%. For comparison, bare Pt-Ni (25:75), RGO/Ni (40 wt % of Ni) and RGO/Pt (40 wt % of Pt) were also synthesized in a similar way.

### 2.3 Instrumentation and measurements

The structural analysis of as-synthesized samples were investigated by X-ray diffraction (XRD) (Philips powder diffractometer PW 3040/60) with Cu  $K\alpha$  radiation ( $\lambda = 1.541 \text{ \AA}$ ). The Fourier transform infrared (FTIR) spectra were recorded on a Magna-IR spectrometer-50 (Nicolet) instrument by a conventional KBr pellet procedure. The Raman scattering was executed on a Lab RAM HR 800 Micro laser Raman system using a 519 nm  $\text{Ar}^+$  laser. XPS measurement was conducted by using an ESCA Probe (MULTILAB from Thermo VG Scientific) with a monochromatic Al  $K\alpha$  radiation (Energy = 1486.6 eV). The morphology of the as-synthesized products was examined by transmission electron microscopy (TEM) using the Phillips-CM 200 electron microscope, operated at 200 kV. The composition of the as-prepared samples was analyzed by an ICP-AES (Prodigy, Teledyne Leeman Labs) and EDX. The magnetic measurements were carried out by a Quantum Design magnetometer (MPMS XL SQUID). The catalytic studies were investigated using an Ultraviolet-visible (UV-Vis) spectrophotometer (Cecil, model no CE3021).

### 2.4 Catalytic study

The reduction reaction of p-nitro phenol by  $\text{NaBH}_4$  has been adopted as a model reaction for the catalytic activity study of as-synthesized Pt-Ni, RGO/Pt, RGO/Ni and RGO/Pt-Ni nanocatalysts (Scheme 1). In a typical procedure, p-nitro phenol (5 mM) and  $\text{NaBH}_4$  (1.5 M) were freshly prepared in milli Q water. For the catalytic study, 2 mL of a  $\text{NaBH}_4$  (1.5 M) solution and 3 mg of each catalyst were mixed with 100 mL of milli Q water. In order to start the reaction, 2 mL of a p-nitro phenol (5 mM) solution was added into the mixture solution. During the reaction process, 1 mL of the reaction solution was taken from the reaction system at a regular interval of 5 minutes, and subsequently, it was diluted with 1 mL of milli-Q water. This was followed by the measuring of the UV-Vis spectra of the solution to examine the concentration of p-nitro phenol by monitoring through the absorption peak at 400 nm.

## 3. Results and discussion

Fig. 1A shows the XRD patterns of RGO, RGO/Pt and RGO/Pt-Ni nanocatalysts. A broadened diffraction peak (002) at 2 theta in the range of 20–30 $^\circ$  (Fig. 1 A (i)) corresponds to the stacked graphene sheets with a short range order.<sup>37</sup> The disappearance of the diffraction peak coming from the disorderedly stacked graphene sheets in all nanocatalysts indicates a reduction of the agglomeration of the RGO sheets. In case of RGO/Pt (Fig. 1A (ii)), the peaks around 40.1 $^\circ$ , 46.6 $^\circ$ , 67.8 $^\circ$ , and 81.9 $^\circ$  are corresponded to the (1 1 1), (2 0 0), (2 2 0), and (3 1 1) planes of Pt face-centered cubic (fcc) crystal structure (JCPDS 04-0802), respectively. This indicates there is a formation of fcc-crystal structured Pt on the RGO. For the RGO/Pt-Ni nanocatalysts, diffraction patterns show the same peaks as above. However, the diffraction peaks are slightly shifted (Fig. 1B) to higher 2 theta values with respect to RGO/Pt and no characteristic peaks of Ni or its oxides are noticed (Fig. 1A (iii)-(v)). The slight shift specifies that Ni atoms have come into the Pt lattice forms solid solution with Pt and Pt-Ni alloys have formed. Fig. 1C shows a linear decrease in the lattice parameter of Pt with an increase of Ni content as

predicted by the Vegard's law; which is also a good signature of the formation of a solid solution (atomic radii of Ni and Pt are 0.124 nm and 0.136 nm respectively). These results suggested

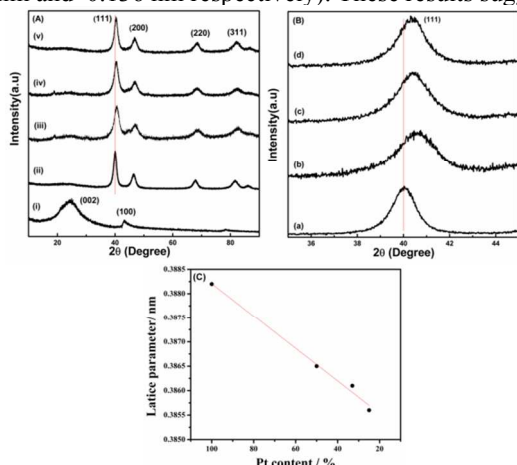


**Fig. 1** (A) XRD patterns of (i) RGO, (ii) RGO/Pt and RGO/Pt-Ni nanocatalysts with Pt/Ni atomic ratios of (iii) 25:75, (iv) 33:67, and (v) 50:50. (B) Pt (111) peak in RGO/Pt-Ni nanocatalysts with the Pt/Ni atomic ratios of 25:75 (curve ii), 33:67 (curve iii), and 50:50 (curve iv) shows shifting towards higher  $2\theta$  values with respect to RGO/Pt (curve i) (C) Lattice parameter of Pt in RGO/Pt and RGO/Pt-Ni nanocatalysts deduced from XRD.

that there is a successful substitute of Pt atoms by Ni atoms, which additionally supports the confirmation of formation of Pt-Ni alloys.<sup>38</sup> It was found from Scherrer equation that the estimated crystallite sizes of Pt-Ni in RGO/Pt-Ni nanocatalysts with atomic ratios 25:75, 33:67 and 50:50 are 4.2, 3.6 and 3.2 nm, respectively.

Moreover, as supporting information, the XRD patterns of the RGO/Ni and Pt-Ni samples are given in Fig. S1. RGO/Ni shows a face-centered cubic (fcc) structure of nickel (JCPDS 04-0802) whereas Pt-Ni (25:75) is also an fcc structure with a small shift of diffraction peaks similar to RGO/Pt-Ni (25:75). This shifting indicates the formation of Pt-Ni alloy.

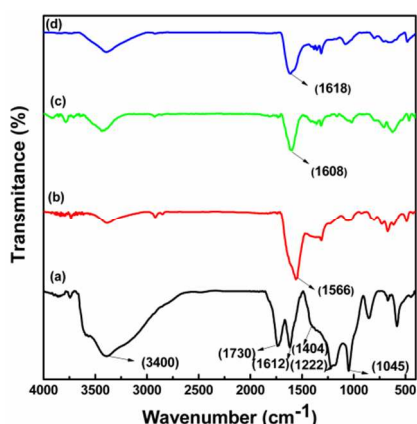


**Fig. 2** FTIR patterns of (a) GO and RGO/Pt-Ni nanocatalysts at Pt/Ni atomic ratios of (b) 25:75, (c) 33:67, and (d) 50:50.

The FTIR spectra of as-synthesized GO and the RGO/Pt-Ni nanocatalysts are compared in Fig. 2. Some characteristic peaks of the oxygenic functional groups of GO in Fig. 2 (a) indicate that graphite successfully undergoes oxidation. Nearly all the characteristic bands of oxygenic functional groups disappear in the FTIR spectra of RGO/Pt-Ni nanocatalysts (Fig. 2 (b)-(d)). It suggests a successfully transformation of GO into RGO in the

reduction process. For RGO/Pt-Ni nanocatalysts, strong absorption band at 1566, 1608 and 1618  $\text{cm}^{-1}$  with Pt/Ni atomic ratios 25:75, 33:67 and 50:50, respectively, can be ascribed to the skeletal vibration of the graphene sheets.<sup>39</sup>

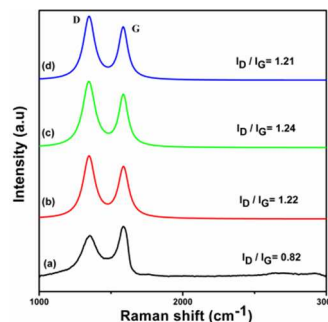


**Fig. 3** Raman spectra of (a) GO and the RGO/Pt-Ni nanocatalysts at Pt/Ni atomic ratios of (b) 25:75, (c) 33:67, and (d) 50:50.

The characteristic Raman spectra of GO and RGO/Pt-Ni nanocatalysts are shown in Fig. 3. Both GO and RGO/Pt-Ni nanocatalysts show the presence of the G and D bands. The intensity ratio ( $I_D/I_G$ ) of the D to the G band is related to the average size of  $\text{sp}^2$  domains.<sup>40</sup> The  $I_D/I_G$  ratio for GO is 0.94 and for RGO/Pt-Ni nanocatalysts with Pt/Ni atomic ratios of 25:75, 33:67 and 50:50 are 1.22, 1.24, and 1.21, respectively. The increase of  $I_D/I_G$  ratios in all RGO/Pt-Ni nanocatalysts, as compared with graphite oxide conclude that the graphite oxide has been successfully deoxygenated and reduced in RGO/Pt-Ni nanocatalysts with different Pt and Ni concentration.

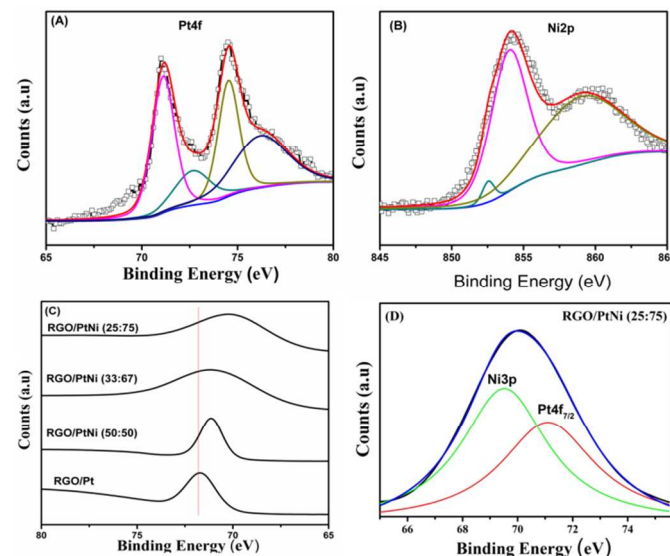


**Fig. 4** The XPS spectra of Pt 4f (panel A) and Ni 2p (panel B) in the RGO/Pt-Ni nanocatalysts at Pt/Ni atomic ratio of 50:50. Panel C shows the Pt  $4f_{7/2}$  peak shift in different nanocatalysts and Panel D shows fitted XPS spectra of Pt  $4f_{7/2}$  in RGO/PtNi (25:75) nanocatalyst (Appearance of Ni 3p spectra).

XPS measurement is used to evaluate the surface structures and chemical states of these RGO/Pt-Ni nanocatalysts. Fig. 4 (A) and (B) show the XPS spectra of Pt 4f and Ni 2p in the RGO/Pt-Ni nanocatalyst with atomic ratio 50:50. It has been observed that Pt exists predominantly in metallic form where as Ni oxidized at the catalytic surface during preparation. A slight negative shifting of Pt  $4f_{7/2}$  peak (Fig. 4(C)) in the RGO/Pt-Ni

nanocatalysts of atomic ratios 50:50, 33:67 and 25:75 with respect to RGO/Pt may be caused by many factors. One of them is transfer of electron from Ni to Pt due to electronegative difference between Ni (1.91) and Pt (2.28). This leads to change in electronic properties of the Pt (lowering the density of state on the Fermi level) in RGO/Pt-Ni nanocatalysts of different atomic ratios.<sup>31</sup> Such change in electronic properties of Pt due to alloying with Ni improves the catalytic performance. For example, it has been reported by several authors<sup>31,41,42</sup> that electron transfer from Ni to Pt may lower the density of states on the Fermi level and decrease the Pt-carbon monoxide (CO) bond energy (weaken the CO adsorption on Pt-Ni alloys) improving the electrocatalytic activity of Pt-Ni alloys toward methanol oxidation. In addition, it has been also observed that with increasing Ni concentration, the Pt  $4f_{7/2}$  peak is getting more broadened. This may be due to the overlap of Ni 3p peak with Pt  $4f_{7/2}$  by increasing the concentration of Ni in the Pt-Ni alloy. It has been reported that the binding energy at 68.9 eV can be assigned to the XPS peak position of Ni 3p.<sup>43,44</sup> When we increase the concentration of Ni, the Ni 3p peak may appear and merge with the Pt  $4f_{7/2}$  peak (as shown in the fitted Fig. 4D). Wakisaka *et al.*<sup>45</sup> has reported that the decrease in electron density at Fermi energy level results in a dull edged XPS peak for Pt-Co and Pt-Ru alloy systems as compared to pure Pt. In our Pt-Ni alloy system, by increasing the Ni concentration, the electron transfer from Ni to Pt enhances which leads to reduction in the density of states at the Fermi level and this may result in the  $4f_{7/2}$  XPS peak broadening.

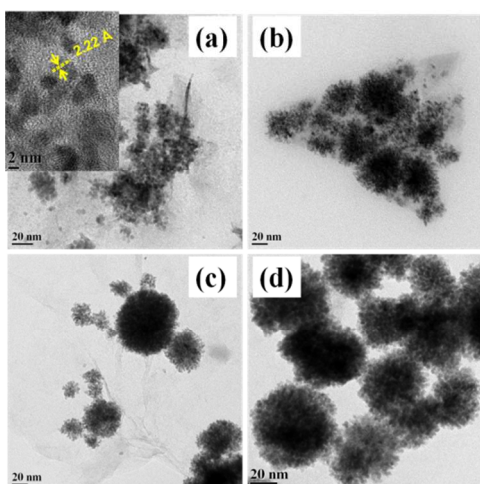


**Fig. 5** TEM images of RGO/Pt-Ni nanocatalysts at Pt/Ni atomic ratios of (a) 25:75, (b) 33:67, (c) 50:50 and (d) bare Pt-Ni nanocatalyst at Pt/Ni atomic ratio 25:75. Inset 2 (a) shows a typical HRTEM image of a portion of a RGO/Pt-Ni nanocatalyst at Pt/Ni atomic ratio 25:75

The morphology and elemental composition of the RGO/Pt-Ni and bare Pt-Ni nanocatalysts were investigated by TEM, EDX, and ICP analysis. The TEM image of RGO/Ni nanocatalyst is shown in Fig. S2 (a) where shows those Ni nanoparticles has higher contrast, visible as dark dots and are spread out uniformly on the reduced graphene sheets. The average particle size is 65 nm. Fig. S2 (b) shows the TEM image of RGO/Pt nanocatalysts. Pt nanoparticles are in nanocluster form with sizes vary from 20 and 80 nm. Higher magnification picture of the RGO/Pt nanocatalyst shows that Pt nanoclusters are the aggregate of several individual Pt nanoparticles of 5 nm size. The TEM images of RGO/Pt-Ni nanocatalysts with different Pt/Ni atomic ratios are shown in Fig. 5 (a)-(c). Each consists of

highly interconnected/aggregated crystalites with an average mean particle diameter of approximately 3-4 nm, which is in good agreement with the value estimated from the XRD data. The particle size was nearly equal for all RGO/Pt-Ni nanocatalysts synthesized with different Pt/Ni atomic ratios. Thus, the effects of the particle size on their magnetic and catalytic activities can be ignored. HRTEM image of the RGO/Pt-Ni (25:75) nanocatalysts is shown as the inset of Fig. 2(a), which reveals the polycrystalline characteristic of the alloy nanoparticles. The lattice spacing of 0.222 nm for (1 1 1) plane of fcc structured Pt-Ni, is larger than that (0.203 nm) of pure Ni.<sup>30</sup> Though, this value is slightly smaller than that of the (1 1 1) plane of Pt (0.23 nm),<sup>46</sup> which may be due to the lattice contraction upon substitution of a Pt atom with a Ni atom. The TEM image of the bare Pt-Ni catalyst (Fig. 5(d)) shows 3-4 nm sized particles are aggregated to form an assemblage of around 50 nm. Size of the assemblage for bare Pt-Ni nanoparticles is higher compare to the RGO incorporated one which results in a lower catalytic activity is discussed later. The loading amount of Pt and Ni (Pt: Ni) in bare Pt-Ni and RGO/Pt-Ni nanocatalysts of different atomic ratios is analyzed by EDX and ICP results and shown in Table 1. The atomic ratios of Ni and Pt determined by the EDX analysis and are consistent with the results obtained by ICP. It is also found from the ICP result that the total amounts of Pt and Ni (Pt+Ni) on RGO sheets are in good agreement with the initial loading amount.

**Table 1.** EDX and ICP-AES results of bare Pt-Ni and RGO/Pt-Ni nanocatalysts of different atomic ratios.

Nanocatalysts	Pt:Ni (EDX)	Pt:Ni (ICP-AES)	PtNi content <sup>a</sup> (wt %)
Pt-Ni (25:75)	24.2:75.8	25.3:74.7	100
RGO/Pt-Ni (50:50)	44.9:55.10	49.1:50.9	37.85
RGO/Pt-Ni (33:67)	33.1:66.9	32.9:67.1	38.05
RGO/Pt-Ni (25:75)	25.3:74.7	24.4:75.6	37.69

<sup>a</sup>The contents of Pt-Ni alloys in the samples were determined by ICP-AES.

The field-dependent magnetic behavior of bare Pt-Ni and RGO/Pt-Ni nanocatalysts with different atomic ratios of Pt and Ni at room temperature (RT, 300 K) and low temperatures (LT, 5 K) are shown in Fig. 6(a) and (b), respectively. At RT and LT, the values of magnetization ( $M$ , at 5 Tesla), remanence ( $M_r$ ), and coercivity ( $H_c$ ) of RGO/Pt-Ni nanocatalysts are listed in Table S1. The magnetization values of RGO/Pt-Ni nanocomposites decreases with the increase of Pt content and is independent of measuring temperature, which is consistent with the result reported in bare Pt-Ni nanostructures.<sup>47</sup> Higher the proportion of Ni, higher is the value of magnetization. From Fig. 6, it is evident that anisotropy is playing an important role here because the room temperature  $M-H$  curves of RGO/Pt-Ni nanocatalysts show definite magnetization, but very small hysteresis and remanence values. But at LT, a large hysteresis and remanence are observed. The magnetization value of the RGO/Pt-Ni nanocatalyst at RT is lower than the reported magnetization values of the Pt-Ni alloy film.<sup>48, 49</sup> This may be attributed to the smaller particle size and the possible presence of the passivating surface layer of metal oxide (NiO) (Formation of NiO at the surface of nanocatalysts conformed by XPS spectra).<sup>27</sup>

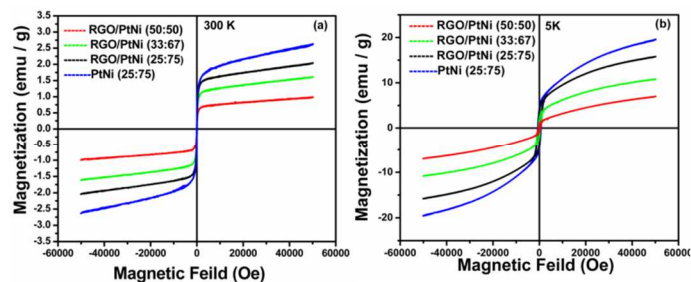


**Fig. 6** Magnetic hysteresis loops of the of Pt-Ni(25:75) and RGO/Pt-Ni nanocatalysts with Pt/Ni atomic ratios of 25:75, 33:67, and 50:50 at (a) 300K and (b) 5 K, respectively.

These studies indicate that at a low temperature the composites are ferromagnetic, but at RT, these demonstrate super paramagnetic behavior. It can be observed that the magnetization value is not saturated even after applying a strong magnetic field (50 KOe) due to the existence of exchange coupling between ferromagnetic Ni and the adjacent anti-ferromagnetic NiO.<sup>50, 51</sup>

### Catalytic properties

The reduction of aromatic nitro compounds to their respective amines by sodium borohydride is very important for the processing of several industrial products. There have been many reports on the catalytic reduction of aromatic nitro compounds using metal, alloys and their composites at a nanoscale, as catalysts.<sup>52-54</sup> In the present study, a comparative study of the catalytic activity of the RGO/Ni, RGO/Pt, Pt-Ni and RGO/Pt-Ni nanocatalysts with different Pt/Ni atomic ratios on the reduction of p-nitro phenol into p-amino phenol by NaBH<sub>4</sub> is undertaken (Scheme 1).

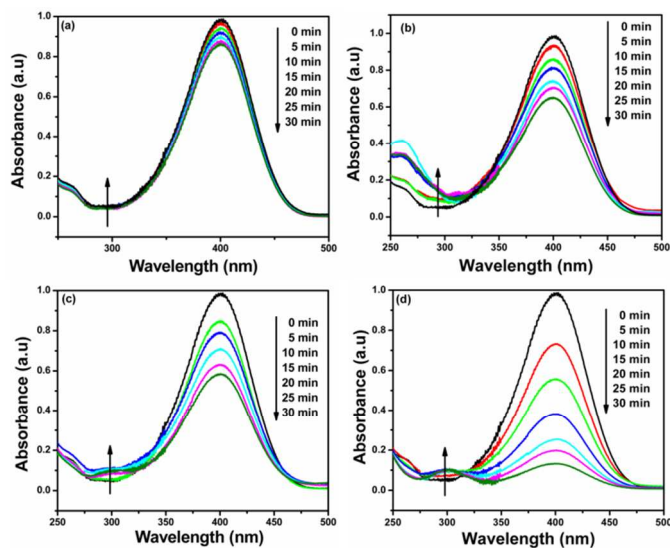


**Fig. 7** UV-vis absorption spectra of the reduction of p-nitro phenol by NaBH<sub>4</sub> in presence of (a) RGO/Ni, (b) RGO/Pt, (c) Pt-Ni (25:75) and (d) RGO/Pt-Ni (25:75) nanocatalysts.

The catalytic reduction took place due to transfer of electron from BH<sub>4</sub><sup>-</sup> (donor) to p-nitrophenol (acceptor) through the nanocatalysts. The rate of electron transfer on the nanocatalysts surface was influenced by three processes: (a) adsorption of p-nitro phenol onto the nanocatalysts surface (b) interfacial electron transfers and (c) desorption of p-nitro phenol left from

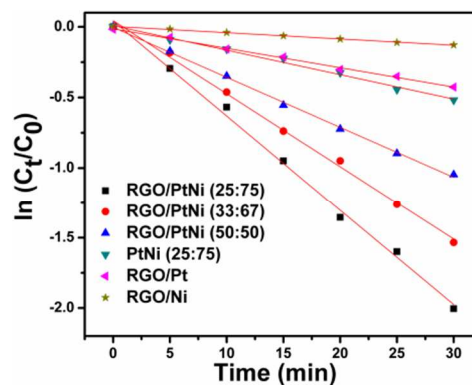
the nanocatalysts surface. Since the both p-nitro phenol and p-amino phenol absorb in the UV-Vis region, so the progress of the reaction is monitored by UV-Vis spectroscopy. It is well known that p-nitro phenol shows a strong absorption peak at 400 nm in an alkaline solution.<sup>55,56</sup> As the reduction reaction proceeds, the intensity of the absorption peak at 400 nm gradually decreases while a new peak appears at 300 nm, which is ascribed to the p-amino phenol. The progress of the reduction process is clearly visible to the naked eye because the yellow color of the p-nitro phenol solution fades out slowly.

Fig. 7 shows the UV-Vis spectra of the diluted reaction solution measured at intervals of 5 minutes using RGO/Ni, RGO/Pt, Pt-Ni (25:75) and RGO/Pt-Ni (25:75) as catalysts. It has been seen that the reduction reaction does not occur in the absence of catalysts or in the presence of pure RGO, even across two days of experimentation. However, in the presence of the catalyst, the absorption due to p-nitro phenol at 400 nm decreases, while there is an increase in the absorption at 300 nm as the reaction proceeds. The absorption at 300 nm corresponds to the formation of p-amino phenol. It is noticed that, compared to RGO/Ni, RGO/Pt and Pt-Ni (25:75) the absorption intensity at 400 nm decreases much faster in the RGO/Pt-Ni (25:75) nanocatalyst as shown in Fig. 7 (a-d), respectively. The conversion (%) of p-nitro phenol to p-amino phenol in 30 min are 12, 33.8, 40, 64.9, 78.4 and 86.5 for RGO/Ni, RGO/Pt, Pt-Ni (25:75), RGO/Pt-Ni(50:50), RGO/Pt-Ni(33:67) and RGO/Pt-Ni (25:75) respectively. The reduction rate of Pt-Ni, RGO/Ni, RGO/Pt and RGO/Pt-Ni nanocatalysts are compared in Fig. 5. It has seen that the reduction rate in RGO/Pt-Ni nanocatalysts are in the following order: RGO/Pt-Ni (50:50) < RGO/Pt-Ni (33:67) < RGO/Pt-Ni (25:75), that is, the catalytic activities increase with an increasing amount of Ni, whereas, RGO/Ni, RGO/Pt, Pt-Ni (25:75) shows a slower reduction rate than RGO/Pt-Ni (25:75) of the same composition.

The kinetics of this reduction reaction was assumed to follow a pseudo-first-order to the concentration of p-nitrophenol when excess NaBH<sub>4</sub> was used.<sup>57, 58</sup> Therefore the kinetic equation of the reduction reaction may be given as follows:

$$kt = \ln C_0 - \ln C = \ln A_0 - \ln A$$

Where C and C<sub>0</sub> are the concentration of p-nitro phenol at time t and t = 0, A and A<sub>0</sub> are the absorbance of p-nitro phenol (at peak of 400 nm) at time t and t=0, respectively; k is the rate constant. The ratio of C<sub>t</sub> to C<sub>0</sub> (C<sub>t</sub>/C<sub>0</sub>) was calculated from the ratio of the absorbances (A<sub>t</sub>/A<sub>0</sub>) at 400 nm. Fig. 8 shows the relation of ln (C<sub>t</sub>/C<sub>0</sub>) versus time (t) in the presence of different catalysts.



**Fig. 8** Plot of ln A<sub>400</sub> vs time for the kinetic studies of the reduction reaction of p-nitro phenol catalyzed by RGO/Ni, RGO/Pt, Pt-Ni and RGO/Pt-Ni nanocatalysts

It is clear from Fig. 8 that  $\ln(C_t/C_0)$  shows a good linear correlation ( $R^2 > 0.99$ ) with the reaction time for all catalysts confirming pseudo-first-order kinetics. The rate constant values are obtained from the pseudo-first-order reaction kinetics (using the slopes of the straight lines of  $\ln(C_t/C_0)$  versus time plot) for different catalysts and are given in Table 2.

The rate constant for the RGO/Pt-Ni nanocatalysts is higher than RGO/Ni and RGO/Pt. This seems to be smaller particle size and the synergetic chemical coupling effects of Pt-Ni alloy, which shows higher catalytic activity compared to monometallic Pt and Ni.<sup>28,32,59</sup> RGO/Pt-Ni (25:75) nanocatalyst shows higher catalytic effect than Pt-Ni (25:75). This indicates that the catalytic activity of a bare Pt-Ni (25:75) can be surprisingly enhanced by compositing it with RGO sheets. Such an enhancement in catalytic activity by compositing with RGO can be ascribed to (1) the adsorption of p-nitro phenol on the surface of RGO through  $\pi$ - $\pi$  stacking interactions that provides a increase in concentration of p-nitro phenol in the vicinity of Pt-Ni (25:75) on RGO/Pt-Ni(25:75) nanocatalyst, leading to strong contact in between them; (2) the increase in local electron concentration by electron transmission from RGO to Pt-Ni (25:75), which causes enhancing the electron-uptake process by p-nitro phenol molecules; and (3) RGO prevents aggregation of Pt-Ni(25:75) nanoparticles and hinder the facile loss of activity.<sup>22,60</sup>

**Table 2** The rate of reduction of p-nitro phenol under different catalysts and the correlation coefficient for  $\ln(C_t/C_0) - t$  plots.

Samples	RGO/Ni	RGO/Pt	Pt-Ni (25:75)	RGO/Pt-Ni (50:50)	RGO/Pt-Ni (33:67)	RGO/Pt-Ni (25:75)
k (X 10 <sup>-3</sup> ) min <sup>-1</sup>	4.4	13.7	17.3	35.5	51.7	67.2
R <sup>2</sup>	0.9968	0.9966	0.9904	0.9985	0.9964	0.9958
TOF <sup>a</sup> (X10 <sup>4</sup> ) molecules g <sup>-1</sup> s <sup>-1</sup>	1.3	3.8	4.5	7.2	8.7	9.6

<sup>a</sup>Reaction condition: p-nitro phenol, 0.01 mmoles; catalysts, 3mg; reaction time, 30 min.

The different rate of reduction of p-nitro phenol with NaBH<sub>4</sub> using RGO/Pt-Ni nanocatalysts of variable compositions of Pt and Ni (atomic ratios 50:50, 33:67 and 25:75) may be attributed to the modified in the electronic structure and the effect of segregation of the materials on the alloy surface. It has been reported that, in the case of the Pt-Ni alloy, the catalytic effect was due to the presence of active sites on Pt, since the surface is enriched with it, whereas, Ni enhances the catalytic effect.<sup>61</sup> The electronic structure of Pt in Pt-Ni matrix is seen to be affected when Ni is added as an alloying element and metal composition affects the electron density ( $n_e$ ) of the alloyed matrix (Pt<sub>x</sub>Ni<sub>1-x</sub>).<sup>62</sup>

$$n_{e, Pt-Ni} = xn_{e, Pt} + (1-x)n_{e, Ni}$$

where 'x' is the atomic fraction of the metallic components in the alloy. Again, by considering the electronegativity, Pt (2.28) is more electronegative than Ni (1.91). This shows that Ni acts as an electron donor while Pt is the acceptor. The increase in the Ni content in the RGO/Pt-Ni nanocatalysts causes electron enrichment on the Pt atom surface, facilitating the transfer process of electrons to the substrate.<sup>32</sup> The catalytic activity appears very sensitive to the presence of RGO as well as to the atomic percentage of the Ni. The turnover number (TON) and the turnover frequency (TOF) of the catalyst are two important factors, which are used for comparing catalyst efficiency. In case of heterogeneous catalysis, the TON is the number of reactant molecules that 1 g of catalyst can convert into products where as TOF is just TON/time.<sup>63</sup> TOF is calculated by using 0.01 mmoles of p-nitro phenol and 3 mg of nanocatalysts for the different nanocatalysts and given in the Table 2.

Furthermore, the magnetic property of the RGO/Pt-Ni nanocatalysts makes it an economical and easy method for separating the catalysts from the reaction system by a strong magnet (Scheme 1).

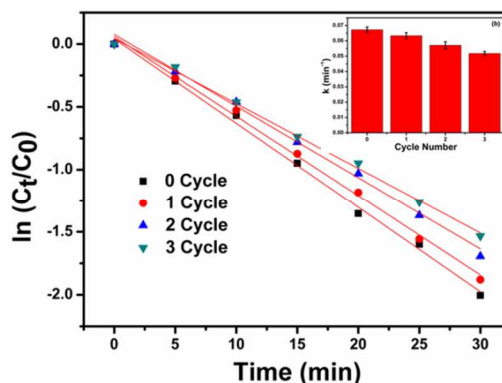


**Fig. 9** Plots of  $\ln(C_t/C_0)$  of p-nitro phenol versus reaction time for successive 3 cycle reactions employing RGO/Pt-Ni (25:75) as catalyst. Inset: Value of rate constant (k) for each cycle with RGO/Pt-Ni (25:75) as catalyst.

The reusability of the bare Pt-Ni (25:75) and RGO/Pt-Ni (25:75) nanocatalysts were tested for reduction of p-nitro phenol by NaBH<sub>4</sub>. It has been seen in RGO/Pt-Ni (25:75) nanocatalyst (Fig. 9) that after the complete of three cycles, the value of rate constant is slightly decreases with increasing cycle. In contrast the rate constant (k) for the bare Pt-Ni (25:75) drops drastically in the second cycle (Fig. S3). These experiments confirm that stability of Pt-Ni (25:75) nanocatalyst was effectively improved by incorporation with RGO sheets. Furthermore RGO sheets as a supporting material could help for preventing aggregation of Pt-Ni (25:75) nanocatalyst and the damage of the RGO/Pt-Ni (25:75) nanocatalyst framework. Therefore the high stability of the catalytic activity is due to the high stability of the RGO/Pt-Ni nanocatalyst.

#### 4. Conclusions

In summary, RGO/Pt-Ni nanocatalysts with different compositions of Pt and Ni were successfully synthesized by a one-step chemical reduction method without using any capping agents. The shift in the XRD peak position of Pt in RGO/Pt-Ni nanocatalysts, as compared to RGO/Pt, confirms formation of Pt-Ni alloy. Magnetic studies reveal a super-paramagnetic-like behavior of RGO/Pt-Ni nanocatalysts at room temperature. The value of the magnetization increases by increasing the concentration of Ni in the RGO/Pt-Ni matrix. In addition, the RGO/Pt-Ni nanocatalysts show superior catalytic activity for the reduction of p-nitro phenol by NaBH<sub>4</sub>. The catalytic performance of RGO/Pt-Ni nanocatalysts was higher than bare Pt-Ni of same composition and is sensitive to the composition of Pt and Ni. The enhanced catalytic performances by synergistic alloying between Pt and Ni on RGO sheets and change in electronic characteristics of the Pt<sub>4f</sub> due to the transfer of electron from Ni to Pt may open up a new approach in the field of advanced catalysts. RGO/Pt-Ni nanocatalysts with good magnetic properties may facilitate the separation of expensive catalyst species from products, by an external magnetic field. It is strongly believed that the as-synthesized nanocatalysts have promising applications in the area of advance catalysts.

## Acknowledgements

We gratefully acknowledge Nano Mission, of Department of Science and Technology, India for the financial support and SAIF and CRNTS, IIT Bombay for providing instrumental facilities.

## Notes and references

<sup>a</sup> IITB-Monash Research Academy, Indian Institute of Technology Bombay, Mumbai-400076, India

<sup>b</sup> Solid State and Structural Chemistry Unit, Indian Institute of Science, Bangalore, 560012

† Electronic Supplementary Information (ESI) available: XRD patterns of RGO/Ni, RGO/Pt and Pt-Ni of atomic ratio 25:75. FTIR patterns of GO and RGO/Pt-Ni nanocatalysts. Raman spectra of GO and the RGO/Pt-Ni nanocatalysts. The XPS spectra of RGO/Pt-Ni nanocatalysts. HRTEM images of RGO/Ni and RGO/Pt nanocatalysts. Plots of  $\ln(C_0/C_t)$  of p-nitro phenol versus reaction time for successive 2 cycle reactions employing bare Pt-Ni (25:75) as catalyst. Table contains room temperature (RT) and low temperature (LT) magnetic data of the RGO-Pt-Ni nanocatalysts of different atomic ratios.

(1) D. Li and R. B. Kaner, *Science*, 2008, **320**, 1170-1171.

(2) X. Huang, X. Qi, F. Boey and H. Zhang, *Chem. Soc. Rev.*, 2012, **41**, 666-686.

(3) C. N. R. Rao, A. K. Sood, K. S. Subrahmanyam and A. Govindaraj, *Angew. Chem. Int. Ed.*, 2009, **48**, 7752-7777.

(4) G. Liao, S. Chen, X. Quan, H. Yu and H. Zhao, *J. Mater. Chem.*, 2012, **22**, 2721-2726.

(5) D. S. Su, J. Zhang, B. Frank, A. Thomas and X. Wang, *ChemSusChem*, 2010, **3**, 169-180.

(6) F. Zeng, Z. Sun, X. Sang, D. Diamond, K. T. Lau, X. Liu and D. S. Su, *ChemSusChem*, 2011, **4**, 1587-1591.

(7) G. Ning, Z. Fan, G. Wang, J. Gao, W. Qian and F. Wei, *Chem. Commun.*, 2011, **47**, 5976-5978.

(8) B. F. Machado and P. Serp, *Catal. Sci. Technol.*, 2012, **2**, 54-75.

(9) J. Pyan, *Angew. Chem. Int. Ed.*, 2011, **50**, 46-48.

(10) A. K. Swain, D. Li and D. Bahadur, *Carbon*, 2013, **57**, 346-356.

(11) K. S. Novoselov, A. K. Geim, S. V. Morozov, D. Jiang, Y. Zhang, S. V. Dubonos, I. V. Grigorieva and A. A. Firsov, *Science*, 2004, **306**, 666-669.

(12) A. Reina, X. T. Jia, J. Ho, D. Nezich, H. B. Son, V. Bulovic, M. S. Dresslhaus and J. Kong, *Nano Lett.*, 2009, **9**, 30-35.

(13) S. Stankovich, D. A. Dikin, R. D. Piner, K. A. Kohlhaas, A. Kleinhammes, Y. Jia, Y. Wu and S. T. Nguyen, *Carbon*, 2007, **45**, 1558-1565.

(14) A. K. Swain and D. Bahadur, *RSC Adv.*, 2013, **3**, 19243-19246.

(15) P. K. Sahoo, B. Panigrahy, S. Sahoo, A. K. Satpati, D. Li and D. Bahadur, *Biosens. Bioelectron.*, 2013, **43**, 293-296.

(16) A. Prakash, S. Chandra and D. Bahadur, *Carbon*, 2012, **50**, 4209-4219.

(17) B. J. Li, H. Q. Cao, J. Shao, M. Z. Qu and J. H. Warner, *J. Mater. Chem.*, 2011, **21**, 5069-5075.

(18) J. H. Zhu, Z. P. Luo and S. J. Wu, *Mater. Chem.*, 2012, **22**, 835-844.

(19) H. K. He and C. Gao, *ACS Appl. Mater. Interfaces*, 2010, **2**, 3201-3210.

(20) X. Y. Yang, X. Y. Zhang, Y. F. Ma, Y. Huang, Y. S. Wang, Y. S. Chen, *J. Mater. Chem.*, 2009, **19**, 2710-2714.

(21) V. Chandra, J. Park, Y. Chun, J. W. Lee, I. C. Hwang and K. S. Kim, *ACS Nano*, 2010, **4**, 3979-3986.

(22) Z. Ji, X. Shen, G. Zhu, H. Zhou and A. Yuan, *J. Mater. Chem.*, 2012, **22**, 3471-3477.

(23) M. J. Hostetler, C. J. Zhong, B. K. H. Yen, J. Anderegg, S. M. Gross, N. D. Evans, M. Porter and R. W. Murray, *J. Am. Chem. Soc.*, 1998, **120**, 9396-9397.

(24) A. Henglein and C. Brancewicz, *Chem. Mater.*, 1997, **9**, 2164-2167.

(25) N. Toshima and Y. Wang, *Langmuir*, 1994, **10**, 4574-4580.

(26) X. Q. Hunag, E. B. Zhu, Y. Chen, Y. J. Li, C. Y. Chiu, Y. X. Xu, Z. Y. Lin, X. F. Duan and Y. Huang, *Adv. Mater.*, 2013, **25**, 2974-2979.

(27) S. Bai, X. Shen, G. Zhu, M. Li, H. Xi and K. Chen, *ACS Appl. Mater. Interfaces*, 2012, **4**, 2378-2386.

(28) J. Yang, X. Shen, G. Zhu, Z. Ji and H. Zhou, *RSC Adv.*, 2014, **4**, 386-394.

(29) Z. Y. Ji, G. X. Zhu, X. P. Shen, H. Zhou, C. M. Wu and M. Wang, *New J. Chem.*, 2012, **36**, 1774-1780.

(30) S. Bai, X. P. Shen, G. X. Zhu, Z. Xu and J. Yang, *CrystEngComm*, 2012, **14**, 1432-1438

(31) Y. Hu, P. Wu, Y. Yin, H. Zhang and C. Cai, *Appl. Catal. B*, 2012, **111**, 208-217.

(32) S. K. Ghosh, M. Mandal, S. Kundu, S. Nath and T. Pal, *Appl. Catal. A: Gen.*, 2004, **268**, 61-66.

(33) J. Huang, S. Vongehr, S. Tang, H. Lu and X. Meng, *J. Phys. Chem. C*, 2010, **114**, 15005-15010.

(34) J. A. Adekoya, E. O. Dare, M. A. Mesubi, A. A. Nejo, H. C. Swart and N. Revaprasadu, *Results in Physics*, 2014, **4**, 12-19.

(35) W. S. Hummers and R. E. Offeman, *J. Am. Chem. Soc.*, 1958, **80**, 1339-1339.

(36) Z. Y. Ji, X. Shen, Y. Song and G. Zhu, *Mater. Sci. Eng. B*, 2011, **176**, 711-715.

(37) Y. C. Si and E. T. Samulski, *Chem. Mater.*, 2008, **20**, 6792-6797.

(38) H. Yang, W. Vogel, C. Lamy and N. Alonso-Vante, *J. Phys. Chem. B*, 2004, **108**, 11024-11034.

(39) Y. Xu, H. Bai, G. Lu, C. Li and G. Shi, *J. Am. Chem. Soc.*, 2008, **130**, 5856-5857.

(40) S. Stankovich, D. A. Dikin, R. D. Piner, K. A. Kohlhaas, A. Kleinhammes, Y. Jia, Y. Wu and S. T. Nguyen, *Carbon*, 2007, **45**, 1558-1565.

(41) K.W. Park, J.H. Choi and Y.E. Sung, *J. Phys. Chem. B*, 2003, **107**, 5851-5856.

(42) Y. Ishikawa, M.S. Liao and C.R. Cabrera, *Surf. Sci.*, 2000, **463**, 66-80.

(43) Y. Ma, R. Wang, H. Wang, V. Linkov and S. Ji, *Phys. Chem. Chem. Phys.*, 2014, **16**, 3593-3602.

(44) J. A. Haber, Y. Cai, S. Jung, C. Xiang, S. Mitrovic, J. Jin, A. T. Bell and J. M. Gregoire, *Energy Environ. Sci.*, 2014, **7**, 682-688.

(45) M. W. S. Mitsui, Y. Hirose, K. Kawashima, H. Uchida and M. Watanabe, *J. Phys. Chem. B*, 2006, **110**, 23489-23496.

(46) H. Zhang, Y. J. Yin, Y. J. Hu, C. Y. Li, P. Wu, S. H. Wei and C. X. Cai, *J. Phys. Chem. C*, 2010, **114**, 11861-11867.

(47) M. Mandal, S. Kundu, T. K. Sau, S. M. Yusuf and T. Pal, *Chem. Mater.*, 2003, **15**, 3710-3715.

## ARTICLE

- (48) R. Krishnan, H. Lassri, S. Prasad, M. Porte and M. Tiessier, *J. Appl. Phys.*, 1993, **73**, 6433-6435.
- (49) Y-S. Kim and S-C. Shin, *Phys.Rev.B*, 1999, **59**, R6597-R6600.
- (50) A. S. Lanje, S. J. Sharma and R. B. Pote, *Arch. Phys. Res.*, 2010, **1**, 49-56.
- (51) B. Li, H. Cao, J. Yin and Y. A. Wu, *J. Mater. Chem.*, 2012, **22**, 1876-1883.
- (52) T. Y. Tu, J. Zeng, B. Lim and Y. N. Xia, *Adv. Mater.*, 2010, **22**, 5188-5192.
- (53) M. Schrunner, M. Ballauff, Y. Talmon, Y. Kauffmann, J. Thun, M. Moller and J. Brey, *Science*, 2009, **323**, 617-620.
- (54) Y. Mei, Y. Lu, F. Polzer, M. Ballauff and M. Drechsler, *Chem. Mater.*, 2007, **19**, 1062-1069.
- (55) S. Praharaj, S. Nath, S. K. Ghosh, S. Kundu and T. Pal, *Langmuir* 2004, **20**, 9889-9892.
- (56) J. Zeng, Q. Zhang, J. Y. Chen, Y. N. Xia, *Nano Lett.*, 2010, **10**, 30-35.
- (57) J. Lee, J. C. Park and H. A. Song, *Adv. Mater.*, 2008, **20**, 1523-1528.
- (58) J. Huang, S. Vongehr, S. Tang, H. Lu and X. Meng, *J. Phys. Chem. C* 2010, **114**, 15005-15010.
- (59) M. Raula, M. H. Rashid, S. Lai, M. Roy, T. K. Mandal, *ACS Appl. Mater. Interfaces*, 2012, **4**, 878-889.
- (60) J. Li, C. Y. Liu and Y. Liu, *J. Mater. Chem.*, 2012, **22**, 8426-8430.
- (61) S. Mukherjee and J. L. Moran-Lopez, *Surf. Sci.*, 1987, **189/190**, 1135-1142.
- (62) M. Treguer, C. de Cointet, H. Remita and J. Khatouri, *J. Phys. Chem. B*, 1998, **102**, 4310-4321.
- (63) S. Saha, A. Pal, S. Kundu, S. Basu and T. Pal, *Langmuir*, 2010, **26**, 2885-2893.